

1 We (the authors) present the original responses in **bold** font while author responses will be in
2 regular font. We indicate the line number where text was added/modified according to the
3 new manuscript. We will type the line number in bold (**L##**) following our response to the
4 comment, while any text which was modified will be in **red**. Our marked manuscript follows.

5 Clark Pennelly and Paul G. Myers

6

7 Reviewer 1

8 **The authors have greatly improved the manuscript compared to the original submission. The**
9 **advantages of the LAB60 simulation over other existing high-resolution simulations of the**
10 **Labrador Sea have been made clear. Additional and revised text, figures and diagrams**
11 **address the comments made by the reviewers before and thus there are only few remaining**
12 **issues to be solved before publication as outlined below in the Specific Comments.**

13 **Specific Comments:**

14 **11-12: This sentence is not really more clear than before. It still gives the impression that your**
15 **regional configuration is set up within the Labrador Sea and the nests are implemented**
16 **therein.**

17 We have modified this sentence to “**Our regional configuration, spanning the full North Atlantic**
18 **and Arctic, includes nested domains within the North Atlantic and Labrador Sea, reducing**
19 computational costs **that** allow for a lengthy simulation **from 2002 to the** near-present time.”.

20 **L11-13**

21

22 **14-16: In the author response you state that you changed this sentence, however it is**
23 **identical to the original manuscript.**

24 We have modified the end of this sentence to be a bit more clear, using your previous
25 recommendation: “We describe the configuration setup and compare against similarly forced
26 lower-resolution simulations to better describe how horizontal resolution impacts the
27 **representation of the Labrador Sea in the model.**”. **L17**

28

29 **168: “with” should probably be “and”.**

30 Fixed; **L176**

31

32 **194:** "configuration" should be "configurations".

33 Fixed. **L203**

34

35 **283:** "LS60" should be "LAB60".

36 Fixed. **L294**

37

38 **352:** "math far closed" should be "are closer" or "match better".

39 Changed to "are closer". **L362**

40

41 **363:** "most" should be "largest".

42 Fixed; **L373**

43

44 **369-372:** In this paragraph you could mention that only data from one cruise is used.

45 **Otherwise on l. 372: during this cruise" the reader does not know which cruise is meant.**

46 We have adjusted this sentence to make it clear that the figure we present is from a single

47 cruise: "When compared against **bottle data collected during a single hydrographic cruise**

48 across Atlantic Repeat Hydrography Line 7 West ...". **382-383**

49

50 **383:** At this point I suggest to clarify that you refer to exchange with the interior basin/central

51 **Labrador Sea.**

52 We have added "with the interior basin" to clarify that there is little exchange between the

53 Labrador Current and the interior Labrador Sea: "Little exchange **with the interior basin** appears

54 to occur along the Labrador Current until the vicinity of Flemish Cap ...". **L397**

55

56 **698:** It seems like the in Fig. 7, the titles for (c) and (d) are wrong. The upper panel should be

57 **Ring A and the lower panel Ring B.**

58 Correct, thanks for catching this. We have fixed the titles for Figure 7 for Ring A and B. **L713**

59

60

61 Introducing LAB60: A 1/60° NEMO 3.6 numerical simulation of the Labrador Sea

62 Clark Pennelly^{1*} and Paul G. Myers¹

63 ¹1-26 Earth Sciences Building, University of Alberta, Edmonton, Alberta, Canada, T6G 2E3

64 *Correspondence to: Clark Pennelly (pennelly@ualberta.ca)

65

66 Abstract

67 A high-resolution coupled ocean-sea ice model is set up within the Labrador Sea. With a
 68 horizontal resolution of 1/60°, this simulation is capable of resolving the multitude of eddies
 69 which transport heat and freshwater into the interior of the Labrador Sea. These fluxes strongly
 70 govern the overall stratification, deep convection, restratification, and production of Labrador
 71 Sea Water. Our regional configuration, spanning the full North Atlantic and Arctic, includes
 72 nested domains within the North Atlantic and Labrador Sea, reducing computational costs that
 73 allow for a lengthy simulation from 2002 to the near-present time. Three passive tracers are
 74 also included: Greenland runoff, Labrador Sea Water produced during convection, and Irminger
 75 Water which enters the Labrador Sea along Greenland. We describe the configuration setup
 76 and compare against similarly forced lower-resolution simulations to better describe how
 77 horizontal resolution impacts the representation of the Labrador Sea in the model.

78

79 1. Introduction

80 The Labrador Sea, between Canada and Greenland, plays a crucial role in the climate
 81 system. Situated between the Canadian Arctic and the North Atlantic, multiple current systems
 82 influence this deep basin. Cold and fresh Arctic water flows south through Fram Strait along
 83 Greenland (de Steur et al., 2009), producing the East Greenland Current (EGC). The EGC flows to
 84 the southern tip of Greenland, merging with warm and salty Irminger Water to become the
 85 West Greenland Current (WGC) before flowing northwards along the western coast (Fratantoni
 86 and Pickart, 2007). The WGC flows cyclonically around the Labrador Sea as well as into Baffin
 87 Bay. Significant amounts of freshwater are supplied to this current system from both Davis
 88 (Cuny et al., 2005; Curry et al., 2011; Curry et al., 2014) and Hudson Strait (Straneo and Saucier,
 89 2008) as it travels around the Labrador Sea. The current system is called the Labrador Current

Deleted: Nested domains within our regional configuration

Deleted: e

Deleted: ,

Deleted: ing

Deleted: that will span

Deleted: over 15 years up

Deleted: the Labrador Sea.

98 where it merges with the outflow from Hudson Strait (Lazier and Wright, 1993). The Labrador
99 Current travels southwards along the eastern coast of North America eventually leaving the
100 Labrador Sea.

101 Numerous eddies are generated throughout the Labrador Sea, both from high lateral
102 density gradients which exist during the convection season (Frajka-Williams et al., 2014) as well
103 as from baroclinic and barotropic instabilities that occur within the boundary currents (Chanut
104 et al., 2008; Gelderloos et al., 2011). The continental slope along the west coast of Greenland
105 has a pronounced change in topography that induces instability of the current system,
106 generating eddies (de Jong et al., 2016). These eddies, known as Irminger Rings, contain a
107 significant amount of freshwater at the surface as well as subsurface heat. Irminger Rings (15-
108 30km radius) typically travel southwestwards into the interior of the Labrador Sea and have a
109 lifespan of up to two years (Lilly et al., 2003). Eddies generated along the Labrador Coast also
110 contain a significant amount of freshwater (Schmidt and Send, 2007; McGeehan and
111 Maslowski, 2011; Pennelly et al., 2019). Regardless of where they are produced, these
112 boundary current eddies often export their properties towards the centre of the basin (Pennelly
113 et al., 2019), influencing the deep convection which occurs. Convective eddies are generated
114 from baroclinic instability which arises from large horizontal density gradients during the
115 convective season (Marshall and Schott, 1999). Convective eddies are much smaller with a
116 radius between 5 and 18 km (Lilly et al., 2003). These eddies are less studied than the other
117 eddy types, partly due to a lack of observations (Lilly et al., 2003) as well as their small size
118 which requires high-resolution models to adequately resolve. Research into the role of each of
119 the above eddies and their role in restratifying the Labrador Sea is still ongoing; there is no
120 consensus on which eddy may be more important, though many have narrowed it down to
121 Irminger Rings and convective eddies (Chanut et al., 2008; Gelderloos et al., 2011; Rieck et al.,
122 2019).

123 Deep convection is a rather rare occurrence, only known to occur at a few places in the
124 ocean. The reason so few places exist is the stringent criteria to produce deep convection: weak
125 stratification that can be enhanced via isopycnal doming as a result of cyclonic circulation, and
126 intense air-sea buoyancy loss (Lab Sea Group, 1998; Marshall and Schott, 1999). Cyclonic

127 circulation and the lateral input of salty Irminger Water helps keep the Labrador Sea weakly
128 stratified. Furthermore, the Labrador Sea experiences strong heat loss during the winter period
129 due to the very cold mid-latitude cyclones which frequent the region (Schulze et al., 2016). The
130 overlying cold and dry air forces a significant flux of heat from the ocean to the atmosphere.
131 This loss of heat promotes the surface layer to increase in density, overturning the weakly
132 stratified water column such that the mixed layer can exceed 2000m in depth (Yashayaev,
133 2007), producing a thick uniform water mass known as Labrador Sea Water (LSW).

134 Once the convective winter ends, the Labrador Sea quickly restratifies itself within 2-3
135 months (Lilly et al., 1999), primarily due to large horizontal density gradients that form
136 convective eddies (Lilly et al., 2003; Rieck et al., 2019) as a result of the deep convection period
137 (Frajka-Williams et al., 2014). The boundary currents continuously shed eddies with relatively
138 buoyant water towards the interior Labrador Sea (Straneo, 2006), increasing stratification. This
139 occurs along the west Greenland and Labrador coasts, though research suggests that the
140 former supplies more freshwater (Myers, 2005; Schmidt and Send, 2007; McGeehan and
141 Maslowski, 2011; Pennelly et al., 2019).

142 LSW is exported out of the Labrador Sea primarily by the Deep Western Boundary
143 Current (Kieke et al., 2009), though it also spreads eastwards at a slower rate. While LSW is the
144 lightest component within the Deep Western Boundary Current, it is one of the water masses
145 which make up the lower limb of the Atlantic Meridional Overturning Circulation (AMOC). As
146 the overturning circulation transports a significant amount of heat and dissolved gasses
147 between the equator and polar regions, changes in the production of deepwater can influence
148 the overturning circulation and ultimately the climate (Bryden et al., 2005). With polar
149 amplification driven by the positive ice-albedo feedback loop, additional freshwater from
150 melted ice enters the EGC and WGC (Bamber et al., 2012). The Labrador Sea is experiencing an
151 increase in freshwater that can be capable of capping convection and preventing LSW from
152 being formed, ultimately reducing the AMOC strength (Böning et al., 2016). However, a non-
153 local increase in the surface freshwater flux may promote AMOC strengthening (Cael and
154 Jansen, 2020) or compensate the local effects of additional freshwater (Latif et al., 2000). Long
155 climate simulations allow investigation into any AMOC regime shifts that shorter, higher-

156 resolution simulations may miss. With such different conclusions, freshwater's influence on the
157 AMOC is not fully known and may vary at different convection regions.

158 While satellite altimetry provides a wealth of information including sea surface height
159 anomalies, geostrophic currents, and waves, hydrographic cruises within the Labrador Sea are
160 often limited to the restratification period when the Labrador Sea is more hospitable for
161 scientific operations. Argo floats, autonomous drifting profilers which can sample down to
162 2000m, have become a popular instrument to acquire in-situ data. However, they still lack
163 coverage within the Labrador Sea which can experience deep convection below their sampling
164 depth (Yashayaev, 2007). Numerical modelling is a useful tool to explore this data-sparse
165 region, though it has its limits. Simulations within the Labrador Sea often experience a drift in
166 model data, producing a Labrador Sea which slowly increases in salinity, and thus density
167 (Treguier et al., 2005; Rattan et al., 2010). Coarse-resolution simulations suffer even further,
168 often overproducing the spatial area of deep convection (Courtois et al., 2017), primarily as a
169 result of not resolving important small-scale features including eddies. These eddies supply the
170 Labrador Sea with significant heat (Gelderloos et al., 2011) and freshwater fluxes (Hátún et al.,
171 2007), both strongly impact the stratification, convection, and production of deep water.
172 Increased horizontal resolution helps produce these eddies and their important fluxes into the
173 interior of the Labrador Sea but numerical drift still is present within high-resolution
174 simulations, albeit reduced in severity (Marzocchi et al., 2015).

175 Numerous high-resolution simulations have been carried out within the North Atlantic.
176 VIKING20X (Rieck et al., 2019), and its predecessor VIKING20, are global $1/4^\circ$ simulations which
177 have a high-resolution $1/20^\circ$ nest. VIKING20X is a multi-decade simulation which is capable of
178 resolving eddies within the Labrador Sea. However, simulations with $1/20^\circ$ horizontal resolution
179 may not resolve sub-mesoscale processes (Su et al., 2018) that can impact stratification by
180 carrying heat and freshwater; higher-resolution is needed. The $1/50^\circ$ HYCOM (Chassignet and
181 Xu, 2017), $1/60^\circ$ NATL60 (Fresnay et al., 2018) and eNATL60 (Le Sommer et al., in prep) provide
182 great insights on the importance of resolving eddies. However, computational expense with
183 such high-resolution simulations is very high, both in computer time and operational costs. This
184 often forces higher-resolution simulations to have a reduced length, perhaps only a few years.

185 The Labrador Sea experiences significant interannual variability (Fischer et al., 2010) and such
186 short simulations may completely miss any connection between LSW production and changes
187 in the AMOC. As such, any high-resolution simulation which is capable of resolving the fine
188 scale features within the Labrador Sea should be carried out for many years to further
189 understand the climate system. Resolving the full North Atlantic at high resolution ($1/60^\circ$) and
190 carrying out a simulation for longer than 10 years would currently be extremely expensive; the
191 above $1/60^\circ$ simulations are 5 or so years in length. However, one can incorporate nested
192 domains to increase horizontal resolution with a relatively minor increase in computing cost.

193 To simulate the Labrador Sea as accurately as possible, we set up a complex numerical
194 configuration which achieves very high resolution within the Labrador Sea while keeping
195 computing costs low such that we will produce over 15 years of simulated data. This simulation
196 will be kept up to near-present time, lagged a few months depending on the availability of
197 forcing data. The high resolution allows for explicit representation of eddies which are crucial to
198 controlling the stratification within the region. We will first describe the model configuration in
199 detail and then compare against similarly-forced lower-resolution simulations to understand
200 how changes in horizontal resolution impacts model results in the Labrador Sea.

201

202 2. Methods

203 The numerical model used for our high-resolution simulation is the Nucleus for
204 European Modelling of the Ocean (NEMO; Madec, 2008), version 3.6, which is coupled to a sea-
205 ice model, LIM2 (Fichefet and Maqueda, 1997). The $1/4^\circ$ Arctic Northern Hemisphere Atlantic
206 configuration (ANHA4; Fig 1a) is used and includes a double nest via the Adaptive Grid
207 Refinement in FORTRAN package (AGRIF; Debreu et al., 2008). The AGRIF software allows for
208 high-resolution nests to communicate along their boundaries, passing information back and
209 forth between domains. The parent ANHA4 domain extends from Bering Strait, though the
210 Arctic and North Atlantic, to 20°S in the South Atlantic. The parent domain's nest uses a spatial
211 and temporal refinement factor of three, bringing resolution to $1/12^\circ$ and the time step to 240s
212 (Table 1) in the North Atlantic Sub Polar Gyre domain (SPG12; Fig 1b). An ANHA4 configuration
213 with a SPG12 nest has been evaluated before by investigating how model resolution influences

214 Labrador Sea Water formation (Garcia-Quintana et al., 2019) as well as eddy formation and
215 eddy fluxes in the North Atlantic Current (Müller et al., 2017; Müller et al., 2019). Another nest
216 is implemented within the SPG12 domain, using a spatial and temporal refinement of five,
217 increasing the horizontal resolution from $1/12^\circ$ to $1/60^\circ$ and reducing the time step to 48s
218 within the Labrador Sea (LAB60; Fig 1c). All nests allow two-way communication such that the
219 parent domain supplies boundary conditions while the daughter domain returns interpolated
220 values to all associated parent grid points. All domains have different horizontal grid spacing
221 but they share the same vertical grid which is set to 75 geopotential levels (Fig. 1d) using partial
222 steps (Barnier et al., 2006). This simulation involves three domains (ANHA4, SPG12, and LAB60)
223 although we primarily discuss what occurs within the $1/60^\circ$ nest.

224 A total variance dissipation scheme (Zalesak, 1979) was used in all domains to calculate
225 horizontal advection. A Laplacian operator was used to compute lateral diffusion in all domains,
226 while a bi-laplacian operator was used for lateral momentum mixing. As some model
227 parameters are grid-scale dependent, Table 1 displays these settings. As lateral boundary
228 conditions have been shown to be very important at producing Irminger Rings in high-
229 resolution simulations (Rieck et al. 2019), we used no-slip lateral boundary conditions within
230 the LAB60 domain while the other domains had free-slip conditions. Model mixed layer depths
231 were calculated via the vertical gradient in temperature and salinity (Holte and Talley, 2009) as
232 opposed to a 0.01 kg m^{-3} change in potential density between the surface and the bottom of
233 the mixed layer; the latter method can produce deeper mixed layers than observations suggest
234 (Courtois et al., 2017). Settings not listed in Table 1 indicate that all domains have an identical
235 value or option; some of these important settings are shown in Table 2.

236 Model bathymetry was interpolated from the $1/60^\circ$ ETOPO GEBCO dataset (Amante and
237 Eakins, 2009) to each domain's grid and bathymetric smoothing along nest boundaries was
238 carried out in order to conserve volume where the parent domain supplies boundary conditions
239 to the daughter domain. All domains were initialized from GLORYS1v1 (Ferry et al., 2009), a
240 global reanalysis ocean simulation, at the beginning of 2002. Monthly open boundary
241 conditions (3D T, S, U, V, and 2D SSH and ice values) across Bering Strait and 20° S were
242 supplied to the ANHA4 domain. These boundary conditions were linearly interpolated from

Deleted: with

244 monthly values, overriding the values within the boundary without the use of a sponge layer.
245 Runoff was supplied via Dai et al. (2009) while we also included Greenland runoff as estimated
246 from a surface mass-balance model (Bamber et al., 2012). Without an iceberg model
247 functioning with the AGRIF software, we treated all solid runoff as a liquid, thus capturing the
248 full freshwater mass at the cost of accuracy in the spatial and temporal placement of
249 freshwater emitted from icebergs.

250 Precipitation, shortwave radiation, downward longwave radiation, 2 meter specific
251 humidity, 2 meter temperature, 10 meter meridional and 10 meter zonal winds originally were
252 supplied from the Canadian Meteorological Centre's Global Deterministic Prediction System's
253 Reforecast product (CGRF; Smith et al., 2014). While high in temporal (hourly) and spatial
254 resolution (33 km in the Labrador Sea), we found the air-sea fluxes were slightly too weak to
255 sustain deep convection after 2010. Rather than start completely over, we switched the
256 atmospheric forcing in 2007 (Fig. 2) when LAB60's mixed layer was still similar to observations.
257 Starting on 1 Jan 2007, we used the DRAKKAR Forcing Set 5.2 (DFS; Dussin et al., 2016). DFS
258 supplies data at 3 hour increments for wind, temperature, and humidity, while precipitation
259 and radiation are daily. DFS has a spatial resolution which is approximately 45 km within the
260 Labrador Sea. Our own analysis of the CGRF data showed a 2002-2015 average yearly heat loss
261 of 47 W m^{-2} from the interior Labrador Sea while DFS removed 53 W m^{-2} (Pennelly and Myers,
262 submitted). Increasing the horizontal resolution likely increased the horizontal buoyancy fluxes
263 and rendered the CGRF's air-sea heat loss, which was appropriate in our ANHA4 and ANHA12
264 configurations, inadequate. The decision to swap to DFS was based on its greater heat loss,
265 promoting a better mixed layer depth throughout the Labrador Sea, though a different forcing
266 product will eventually be needed as DFS does not currently extend past 2017. Supplemental
267 Fig. 1 depicts the difference in mixed layer depth between the LAB60 simulation forced by
268 CGRF, when forced with CGRF through 2007 and then forced by DFS, as well as what ARGO
269 observations suggest. The weaker air-sea heat loss as forced by the CGRF product leaves the
270 mixed layer with little interannual variability that doesn't compare well with observations.

271 Early testing showed that adding passive tracers increases the computing resources
272 required by about 20% per passive tracer. To keep the simulation from requiring too many
273 resources, we limited LAB60 to three passive tracers:

- 274 1. Liquid runoff from Greenland
- 275 2. Irminger Water ($T > 3.5^{\circ}\text{C}$, $S > 34.88$) which flows westward past Cape Farwell (Fig. 3b)
- 276 3. Labrador Sea Water ($\sigma_{\theta} > 27.68 \text{ kg m}^{-3}$) formed within the mixed layer of the Labrador
277 Sea (Fig. 3c)

278 Runoff from Greenland was included due to the importance of Greenland's freshwater
279 contribution to changes within the Labrador Sea. Water mass definitions for Irminger Water
280 and Labrador Sea Water were selected based on previous studies (i.e. Kieke et al., 2006; Myers
281 et al., 2007). Note that there is no maximum density criteria given to our Labrador Sea Water
282 tracer- the tracer is formed throughout the water column until it reaches the bottom of the
283 mixed layer. Figure 3 illustrates both the source regions as well as the tracer extent as of 1 Jan
284 2010. While these water masses have been studied before (Kieke et al., 2006; Myers et al.,
285 2007; Böning et al., 2016), there has been no attempt to use them as passive tracers at a
286 resolution higher than $1/20^{\circ}$ (Böning et al., 2016).

287 The LAB60 simulation originally started on the Graham cluster of Compute Canada.
288 Other high-resolution simulations often use thousands of computer processors but our
289 simulation could not run on more than 672 CPUs on this cluster as it would stall during domain
290 construction. The years 2002-2007 were carried out on Graham, after which a new allocation
291 on a different high performance Compute Canada cluster, Niagara, became available to us. The
292 LAB60 simulation on Niagara did not suffer from the same issue as it did on Graham and we
293 were able to use many more processors. Initial testing found a substantial increase in the
294 number of days simulated per job submission when the number of CPUs was increased from
295 672 to 3000; tests using 4000 CPUs showed no further improvement. Thus, we carried out the
296 remainder of the LAB60 simulation with 3000 CPUs. Each job submission required around 22
297 hours to carry out, providing 40 days of model output. The real time to finish each 40 day
298 submission naturally varied across the year, increasing during winter which we attribute to the
299 sea-ice model.

300 A spin-up period (Fig. 2) was required as the model quickly went unstable and crashed.
301 We attribute this to the interpolation of the $1/12^\circ$ GLORYS1v1 data onto the LAB60 grid; the
302 resulting data were not smooth enough and numerical noise was generated, leading to model
303 failure. To reduce this noise, a gradual spin-up procedure took place. First, we kept the
304 numerical timestep very low (2s in LAB60) when the model was initialized. We also set the
305 $1/60^\circ$ nests' eddy viscosity and diffusivity values to be equal to those within the SPG12 nest.
306 We gradually increased the timestep and reduced the viscosity and diffusivity values over the
307 first year (2002) to what is within Table 1. Other than also increasing the timestep to stay in line
308 with LAB60, no other values were changed across the coarser ANHA4 and SPG12 domains. To
309 allow LAB60 to adjust to the final settings, we consider the 2003 year to be an adjustment year
310 (Fig. 2).

311 To assess the validity of LAB60, model results were compared against AVISO satellite
312 data (<https://www.aviso.altimetry.fr/>), specifically U/V geostrophic velocities which are derived
313 from the sea surface height. Argo profiler data (<http://www.argo.net/>) was also used to assess
314 the mixed layer. Bottle data from cruise 18HUD20080520, accessed from CCHDO
315 (<https://cchdo.ucsd.edu/cruise/18HU20080520>) on 10 April 2018 was used to compare
316 observations across the AR7W section.

317

318 3. Model Simulation Results

319 To understand what is gained by resolving the Labrador Sea at $1/60^\circ$, we compare the
320 output of our LAB60 simulation with similarly forced ANHA simulations at both $1/4^\circ$ (ANHA4)
321 and $1/12^\circ$ (ANHA12). The large-scale circulation (top 50m) is shown for our 3 simulations (Fig. 4)
322 as well as AVISO geostrophic velocities. All simulations have greater speed within the West
323 Greenland Current (ANHA4: up to 0.8; ANHA12: 0.8; LAB60: 0.6; AVISO: 0.4 m s^{-1}) and Labrador
324 Current (ANHA4: up to 0.6; ANHA12: 0.6; LAB60: 0.4; AVISO: 0.4 m s^{-1}) as altimetry observations
325 suggest slower speeds here. However, Lin et al., (2018) found maximum speed up to 0.74 m s^{-1}
326 along the west coast of Greenland. Both the ANHA4 and ANHA12 configuration have larger
327 values further up the western coast of Greenland, as well as connecting the West Greenland
328 Current and the Labrador Current; features that do not occur in both LAB60 and observations.

329 As LAB60 and observations have less average speed occurring within these boundary currents,
 330 we suspect that all configurations have some large differences in eddy activity, particularly
 331 where these boundary currents are.

332 Eddy kinetic energy (EKE: $0.5(\overline{U_g'^2} + \overline{V_g'^2})$, Fig. 5) was calculated from geostrophic
 333 velocity anomaly based on the sea level anomaly (SLA) from the 2004-2013 mean state:

$$U_g' = -\frac{g SLA}{f \Delta y}$$

$$V_g' = -\frac{g SLA}{f \Delta x}$$

334 where g is the gravitational constant, f is the Coriolis parameter, and Δy and Δx are model grid
 335 length. Overbars indicate the 2004-2013 mean value while primed variables indicate a deviation
 336 from the mean state. AVISO observations were already supplied as geostrophic velocities.
 337 High levels of EKE can be found along the west coast of Greenland (Fig. 5), extending into the
 338 interior of the basin around 62° N, as well as along the Labrador coast's shelf break. The path
 339 extending from the west coast of Greenland is mostly due to Irminger Rings which leave this
 340 coast and travel westward (Chanut et al., 2008). While the EKE extending from west Greenland
 341 enters the interior of the Labrador Sea, that which stems from the Labrador coast does not
 342 penetrate far into the interior. The ANHA4 simulation has low EKE along the west coast of
 343 Greenland (around $100 \text{ cm}^2 \text{ s}^{-2}$) and along the Labrador Coast's shelf break ($10\text{-}30 \text{ cm}^2 \text{ s}^{-2}$). The
 344 ANHA12 simulation shows improvement, having much higher EKE extending from west
 345 Greenland ($100\text{-}300 \text{ cm}^2 \text{ s}^{-2}$) however the EKE does not quite extend into the interior of the
 346 Labrador Sea but instead remains in the northern Labrador Sea. Furthermore, there is
 347 additional EKE along the Labrador shelf break ($30\text{-}50 \text{ cm}^2 \text{ s}^{-2}$) compared against ANHA4. The
 348 LAB60 simulation shows further improvement as the EKE signature from the west Greenland
 349 coast is greater ($100\text{-}1000 \text{ cm}^2 \text{ s}^{-2}$) and now enters into the interior of the Labrador Sea. A
 350 notable increase in EKE also occurs along the Labrador shelf break ($100\text{-}200 \text{ cm}^2 \text{ s}^{-2}$) and within
 351 the interior Labrador Sea ($10\text{-}100 \text{ cm}^2 \text{ s}^{-2}$). LAB60 matches well against observations along the
 352 west coast of Greenland and the Labrador shelf break (both above $1000 \text{ cm}^2 \text{ s}^{-2}$) as well as the
 353 interior Labrador Sea ($10\text{-}100 \text{ cm}^2 \text{ s}^{-2}$). LAB60's higher interior EKE may be partially from
 354 convective eddies that are formed during the wintertime. However, LAB60 has lower EKE within

Deleted: s

356 the Northwest Corner where ANHA4, ANHA12, and the observations exceed $1000 \text{ cm}^2 \text{ s}^{-2}$ over a
 357 wide area. LAB60 matches the spatial distribution albeit with reduced EKE.

358 The differences in the EKE field between these configurations identify that each
 359 simulation is resolving features of varying spatial scales. The ANHA4 simulation, with low EKE
 360 within the Labrador Sea, does not adequately resolve eddies in this region, as illustrated with a
 361 snapshot of normalized model relative vorticity (Fig. 6). However, the larger scale meanders
 362 within the North Atlantic Current are visible. ANHA12 shows a greater degree of mesoscale
 363 features (50 to 500 km), though distinct eddies within the Labrador Sea are also not resolved.
 364 LAB60 resolves eddies along both the west coast of Greenland as well as the Labrador Coast. A
 365 video showing LAB60's normalized relative vorticity is shown in Supplementary Video 1.

366 A few Irminger Rings are shown in Fig. 7, a snapshot in time from 26 July 2007. A newly
 367 spawned ring (Fig. 7c) shows very strong surface speeds (up 0.6 m s^{-1} for Ring A; Fig. 7a) while
 368 older eddies to the south have reduced speeds (up to 0.3 m s^{-1} for Ring B; Fig. 7a). To
 369 investigate the stratification strength, we calculate the amount of energy needed to produce a
 370 neutrally stratified column extending down to some reference depth, h . This proxy, called
 371 convective energy, is given by:

$$\text{Convective energy}(h) = \frac{g}{\text{Area}} \iint \left[h \rho_{\theta}(h) - \int_0^h \rho_{\theta}(z) dz \right] dA$$

372 where g is the gravitational constant, Area is the total surface area over our region of interest
 373 (Fig. 1c), h is the reference depth (2000m used in this study), $\rho_{\theta}(z)$ and $\rho_{\theta}(h)$ are the potential
 374 density at each grid cell and the potential density of the grid cell at the reference depth, and A
 375 is the surface area of each grid cell. A strongly stratified column of water corresponds to a high
 376 convective energy value. A snapshot of convective energy (Fig. 7b) shows that most of these
 377 eddies have substantially higher amounts compared to the background Labrador Sea,
 378 suggesting that the cool and fresh WGC water, as well as warm and salty Irminger Water keep
 379 these eddies strongly stratified. However, these eddies age within the Labrador Sea, and while
 380 a new eddy has strong stratification ($>3000 \text{ J m}^{-3}$), an eddy which has evolved over many
 381 months (Fig. 7d) has weaker stratification (about 2000 J m^{-3}). Older eddies may have very weak
 382 stratification as they may have experienced two convective winter periods of buoyancy

383 removal. This has been noted before, as Lilly et al. (2003) found aged Irminger Rings with a
384 mixed layer that surpassed 1000m.

385 These differences in resolving the mesoscale (50 to 500 km) and sub-mesoscale (<50
386 km) processes within each simulation produced significant changes within the Labrador Sea as
387 seen from modeled convective energy values as averaged from 2004-2013 (Fig. 8). Resolving
388 few eddies, the ANHA4 simulation's interior Labrador Sea lacks the buoyancy flux and remains
389 very weakly stratified across a wide region. The ANHA12 simulation partially resolves some
390 mesoscale features and eddy fluxes from the Greenland coast which supplies buoyancy to the
391 Northern Labrador Sea and has higher convective energy. Furthermore, the spatial extent of
392 the weakly stratified region has shrunk and resides primarily within the Labrador Sea, as
393 opposed to ANHA4 which spills out of the basin. LAB60, fully capable of resolving buoyant
394 eddies from the Greenland and Labrador coast, as well as convective eddies, has a much
395 stronger degree of stratification in the interior region. A visible path of strong stratification
396 appears around 60°N along this coastline, eventually extending away from the coastline around
397 62°N. This path is consistent with the general path that simulated Irminger Rings take (Chanut
398 et al., 2008). Supplemental Video 2 shows the convective energy of the LAB60 simulation from
399 2004 through the end of 2013.

400 The ANHA4 simulation experiences weaker stratification in the Labrador Sea than
401 ANHA12 and LAB60, driving a deeper maximum mixed layer that also covers a larger spatial
402 extent (Fig. 9). However, the maximum mixed layer depth as simulated by ANHA4 and ANHA12
403 greatly exceed what Argo observations suggest (Fig. 9d). ANHA12 has higher EKE within the
404 WGC, supplying more buoyancy to the northern portion of the Labrador Sea, reducing both the
405 vertical extent of the mixed layer as well as the spatial extent where the mixed layer is deeper
406 than 1000m. LAB60 has higher EKE than ANHA12, and the vertical and spatial extent of deep
407 mixing is reduced even further. LAB60's mixed layer is far more similar to what ARGO
408 observations suggest, suggesting the additional eddy fluxes to be fairly accurate. The evolution
409 of LAB60's mixed layer depth is shown in supplemental video 3 from 2004 through the end of
410 2013.

411 After the bottom of the mixed layer returns to the near-surface, a newly formed LSW
 412 mass is left behind. To account for density drift, we allow the LSW classification to evolve in
 413 time, unlike our LSW passive tracer. We calculated LSW density and thickness by binning by
 414 potential density, referenced to 1000 dbar, with bin lengths of 0.001 kg m^{-3} . This was carried
 415 out within the black outlined polygon in Fig 1c for each daily output file per year. The density
 416 bin which had the thickest layer across the year was set as the maximum density of LSW for
 417 that year. The minimum density was defined to be 0.02 kg m^{-3} less than the maximum density.
 418 Linear interpolation occurred between years to allow for a gradual shift in density to prevent
 419 staircase patterns from emerging. Large differences in both the density as well as the thickness
 420 are present between the simulations shown in Fig. 10. The ANHA4 and ANHA12 simulations
 421 have similar density values of LSW while the LAB60 simulation is less dense. While the
 422 interannual variability matches fairly well across all configurations, the density values suggested
 423 by LAB60 are closer to ARGO observations (32.34 to 32.36 kg m^{-3} ; Yashayaev and Loder, 2016)
 424 during the same time period. We suspect the denser LSW formed by ANHA4 and ANHA12 is
 425 primarily attributed to the lack of buoyancy coming from Greenland. As similar air-sea heat
 426 losses should occur in all three configurations, the weaker stratification of ANHA4 and ANHA12
 427 indicates that deep mixing is more likely producing not only a denser LSW layer, but also a
 428 thicker one. Yashayaev and Loder (2016) also investigated the thickness of LSW (their Fig. 8),
 429 and while our simulations do not quite capture the same interannual variability and amplitude
 430 suggested their analysis using ARGO profilers, LAB60 is far more accurate than the lower-
 431 resolution configurations.

Deleted: match

Deleted: far

432 All simulations encounter some degree of numerical drift within the Labrador Sea (Fig.
 433 11), judging from the salt and heat content change as calculated between the surface and
 434 seafloor within the polygon in Figure 1 since 2004. ANHA4 experiences the largest drift in both
 435 salt and heat, helping us understand why LSW is so dense in this simulation. ANHA12 also
 436 experiences drift, though slightly less severe. LAB60 has a small but gradual increase in both salt
 437 and heat content although it is difficult to state if this is drift or simply interannual to decadal
 438 variability. Regardless of the cause, LAB60's change in both heat and salt content is very
 439 minimal compared against the lower-resolution simulations.

Deleted: most

443 When compared against bottle data collected during a single hydrographic cruise across
 444 Atlantic Repeat Hydrography Line 7 West (AR7W; Fig 12), LAB60 is slightly warmer (about 0.25
 445 °C) and saltier (about 0.05 kg m⁻³) throughout the interior. This causes LAB60 to be slightly
 446 denser with isopycnals residing higher than observations during this cruise suggest.
 447 Observations were not carried out above Greenland's continental slope, although they show
 448 some presence of the warm core of the WGC which the model captures. Salinity values close to
 449 the Labrador coast compare well while LAB60 is slightly warmer (about 0.5 °C) above the
 450 continental shelf.

Deleted: observations

Deleted: the

451 The three passive tracers implemented within the full LAB60 configuration (Fig. 3) show
 452 where Greenland runoff, Irminger Water, and Labrador Sea Water travel to. These tracers were
 453 selected because they either contain a significant amount of buoyant water compared to the
 454 Labrador Sea, or are produced via convection in the Labrador Sea. From this image on 1 Jan
 455 2010, we see a large portion of Greenland's runoff (Fig. 3a) resides within Baffin Bay as well as
 456 along the Labrador Coast. Some of this tracer is present where the ocean depth is greater than
 457 2000m. A few Irminger Rings are identifiable, due to their thicker freshwater cap, which are in
 458 water deeper than 3000m. Little exchange with the interior basin appears to occur along the
 459 Labrador Current until the vicinity of Flemish Cap, after which a significant portion of the tracer
 460 propagates eastward. Supplemental Video 4 shows this the evolution of this tracer from 2004
 461 through the end of 2013.

462 Irminger Water ($T > 3.5^{\circ}\text{C}$, $S > 34.88$; Fig. 3b) which flows west past Cape Farwell, enters
 463 the interior Labrador Sea with the greatest amounts where the seafloor is at a depth between
 464 2000 and 3000m. Similar as above, individual Irminger Rings are visible, containing a larger
 465 amount of Irminger Water than the surrounding water. This water mass also flows along the
 466 Labrador Coast until it is in the vicinity of Flemish Cap. Supplemental Video 5 shows this the
 467 evolution of this tracer from 2004 through the end of 2013.

468 Our Labrador Sea Water tracer (Fig. 3c) is traced where the mixed layer produces water
 469 with a potential density above 1027.68 kg m⁻³ within the black contour identified in the figure.
 470 This definition differs compared to our method of classifying LSW as we did not implement any
 471 FORTRAN code to detect and compensate for density drift of our simulation, instead sticking to

474 a strict density classification for this tracer. As this image was made at the start of the
475 convection season, the current deep patch is a freshly produced layer that reaches up to 800m
476 deep. After forming, LSW spreads southwards along the Labrador shelf break as well as to the
477 southeast. Supplemental Video 6 shows this the evolution of this tracer from 2004 through the
478 end of 2013.

479 4. Discussion

480 We describe a 10+ year long, high-resolution simulation which achieves $1/60^\circ$ horizontal
481 resolution in the Labrador Sea via two nests inside a regional configuration, resolving mesoscale
482 and sub-mesoscale processes which strongly impact the deep convection which occurs here.
483 We show that lower-resolution simulations fail to resolve these key processes that strongly
484 control the production of Labrador Sea Water, an important water mass within the Atlantic
485 Meridional Overturning Circulation. While the NATL60 and eNATL60 simulations were designed
486 with the SWOT altimetry satellite mission in mind (NATL60 website: [https://meom-](https://meom-group.github.io/swot-natl60/virtual-ocean.html)
487 [group.github.io/swot-natl60/virtual-ocean.html](https://meom-group.github.io/swot-natl60/virtual-ocean.html)), their integration period, like many other high-
488 resolution simulations, is a handful of years. LAB60, although covering a much smaller region,
489 could be a valuable asset to many users who require a lengthy period of high-resolution model
490 output. We also have included three passive tracers which are often excluded in simulations at
491 this resolution. Our three passive tracers highlight regions where each water mass enters the
492 interior region of the Labrador Sea, demonstrating the pathways of buoyant Greenland melt
493 and Irminger water. Furthermore, we trace Labrador Sea Water which is formed during the
494 convective winter period.

495 We show that LAB60 has greater EKE than our lower-resolution simulation, resolving
496 eddy fluxes including Irminger Rings, boundary current eddies, and likely convective eddies as
497 indicated by greater EKE within the interior. Boundary current eddies still appear relatively
498 disconnected from the interior basin, adding further support that these eddies have limited
499 influence on convection and restratification (Rieck et al., 2019). We offer no additional support
500 regarding the relative importance of Irminger Rings and convective eddies on controlling deep
501 convection; this is currently being investigated for a later manuscript. Model drift appears very
502 low, a large improvement over the ANHA4 and ANHA12 configurations. The drift might produce

503 slightly denser LSW than observations suggest, however LAB60s density is much more accurate
504 than ANHA4 and ANHA12. The boundaries of LAB60, supplied by the inner SPG12 nest, may
505 influence the high-resolution nest. We note that the North Atlantic Current, which is close to
506 the boundary, has less EKE and vorticity than the ANHA4 and ANHA12 simulations. Conversely,
507 the WGC close to the eastern nested boundary has multiple jets which have been noted in
508 hydrographic data (Pickart, personal communication). Boundary communication is always a
509 concern in nested simulations and LAB60 is no different. More investigation will reveal any
510 potential boundary issues but our results so far indicate no further areas of potential concern.

511 Others have investigated the Labrador Sea using numerical simulations with different
512 resolution. Böning et al. (2016) traced Greenland meltwater with the 1/20° VIKING20 and 1/4°
513 ORCA025 simulations, noting more meltwater entered the interior Labrador Sea at higher
514 resolution partially as a result of greater WGC eddy fluxes but not from the Labrador coast. The
515 minor amount of eddy fluxes from the Labrador coast has been noted earlier even at lower
516 resolution (1/3°; Myers, 2005). Steadily increasing horizontal resolution has so far not changed
517 this for the Labrador coast, though this is opposite for the WGC. LAB60 has a clear increase in
518 EKE and likely greater eddy fluxes from the WGC into the interior of the Labrador Sea.

519 We have many ambitious research topics which we plan to use LAB60 to investigate.
520 This includes, but is not limited to, the variability and structure of the West Greenland Coastal
521 Current, Labrador Sea Water production, and the role of both Irminger Rings and convective
522 eddies in controlling stratification in the Labrador Sea. This lengthy high-resolution simulation
523 with three passive tracers will provide valuable information for many numerical studies within
524 the Labrador Sea for years to come.

525

526 Code and/or data availability

527 The FORTRAN code used to carry out the LAB60 simulation can be accessed from the
528 NEMO version 3.6 repository
529 (<https://forge.ipsl.jussieu.fr/nemo/browser/NEMO/releases/release-3.6>). A few FORTRAN files
530 were modified to handle our passive tracers. The complete FORTRAN files as well as the
531 CPP.keys, namelists, and associated files can be found on Zenodo (Pennelly, 2020). Initial and

532 boundary conditions, atmospheric forcing, and numerical output were too large to host on a
533 repository and instead are hosted on our lab's servers as well as the Compute Canada Niagara
534 server. These data can be requested by emailing the corresponding author.

535

536 Author Contribution

537 PM designed the layout of the LAB60 configuration which included the region of
538 interest, numerical length, and which forcing and initial conditions to supply, as well as
539 supervised CP. CP produced the configuration, modified the FORTRAN code, set up the
540 configuration on the high-performance computing systems, carried out the simulation, and
541 performed the analysis. The manuscript was prepared by CP with contributions by PM.

542

543 Acknowledgements

544 The authors would like to thank the NEMO development team as well as the DRAKKAR
545 group for providing the model code and continuous guidance. We express our thanks to
546 Westgrid and Compute Canada (<http://www.computecanada.ca>) for the computational
547 resources to carry out our numerical simulations as well as archival of the experiments. We
548 would like to thank Nathan Grivault for his help to migrate our configuration between
549 computing clusters, as well as Charlene Feucher for her help with ARGO data. This work was
550 supported by an NSERC Climate Change and Atmospheric Research Grant (Grant RGPCC
551 433898) as well as an NSERC Discovery Grant (Grant RGPIN 04357).

552

553 The authors declare that they have no conflict of interest.

554

555

556 References

557 Amante, C. and Eakins, B.W.: ETOPO1 1 Arc-minute global relief model: procedures data
558 sources and analysis. NOAA Technical Memorandum NESDIS, NGDC-24 19, 2009.
559 Bacon, S., Gould, W.J., and Jia, Y.: Open-ocean convection in the Irminger Sea. Geophysical
560 Research Letters, 30(5), 2003.

561 Bamber, J., van den Broeke, M., Ettema, J., Lenaerts, J., and Rignot, E.: Recent large increases in
562 freshwater fluxes from Greenland into the North Atlantic. *Geophysical Research Letters*, 39(19),
563 2012.

564 Barnier, B., Madec, G., Penduff, T., Molines, J.-M., Treguier, A.-M., Le Sommer, J., Beckmann, A.,
565 Biastoch, A., Böning, C., Dengg, J., Derval, C., Durand, E., Gulev, S., Remy, R., Talandier, C.,
566 Theetten, S., Maltrud, M., McClean, J., and De Cuevas, B.: Impact of partial steps and
567 momentum advection schemes in a global ocean circulation model at eddy permitting
568 resolution. *Ocean Dynamics*, 56 (5-6), 543-567, 2006.

569 Böning, C.W., Behrens, E., Biastoch, A., Getzlaff, K., and Bamber, J.L.: Emerging impact of
570 Greenland meltwater on deepwater formation in the North Atlantic Ocean. *Nature Geoscience*,
571 9(7), 523, 2016.

572 Brossier, C.L., Léger, L., Giordani, H., Beuvier, J., Bouin, M.N., Ducrocq, W., and Fourrié, N.:
573 Dense water formation in the north-western Mediterranean area during HyMeX-SOP2 in 1/36°
574 ocean simulations: Ocean-atmosphere coupling impact. *Journal of Geophysical Research:*
575 *Oceans*, 122(7), 5749-5773, 2017.

576 Bryden, H.L., Longworth, H.R., and Cunningham, S.A.: Slowing of the Atlantic meridional
577 overturning circulation at 25°N. *Nature*, 438(7068), 655, 2005.

578 Cael, B.B. and Jansen, M.F.: On freshwater fluxes and the Atlantic meridional overturning
579 circulation. *Limnology and Oceanography*, 5(2), 185-192, 2020.

580 Chanut, J., Barnier, B., Large, W., Debreu, L., Penduff, T., Molines, J.M., and Mathiot, P.:
581 Mesoscale eddies in the Labrador Sea and their contribution to convection and restratification.
582 *Journal of Physical Oceanography*, 28(8), 1617-1643, 2008.

583 Chassignet, E.P. and Xu, X.: Impact of horizontal resolution (1/12 to 1/50) on Gulf Stream
584 separation, penetration, and variability. *Journal of Physical Oceanography*, 47(8), 1999-2021,
585 2017.

586 Courtois, P., Hu, X., Pennelly, C., Spence, P., and Myers, P.G.: Mixed layer depth calculation in
587 deep convection regions in ocean numerical models. *Ocean Modelling*, 120, 60-78, 2017.

588 Cuny, J., Rhines, P.B., and Kwok, R.: Davis Strait volume, freshwater and heat fluxes. *Deep Sea*
589 *Research Part I: Oceanographic Research Papers*, 52.3, 519-542, 2005.

590 Curry, B., Lee, C.M., and Petrie, B.: Volume, freshwater, and heat fluxes through Davis Strait,
591 2004-05. *Journal of Physical Oceanography*, 41(3), 429-436, 2011.

592 Curry, B., Lee, C.M., Petrie, B., Moritz, R.E. and Kwok, R.: Multiyear volume, liquid freshwater,
593 and sea ice transports through Davis Strait, 2004-10. *Journal of Physical Oceanography*, 44(4),
594 1244-1266, 2014.

595 Dai, A., Qian, T., Trenberth, K.E., and Milliman, J.D.: Changes in continental freshwater
596 discharge from 1948 to 2004. *Journal of Climate*, 22(10), 2773-2792, 2009.

597 Debreu, L., Vouland, C., and Blayo, E.: AGRIF: Adaptive grid refinement in Fortran. *Computers
598 and Geosciences*, 34(1), 8-13, 2008.

599 Dussin, R., Barnier, B., and Brodeau, L.: The making of Drakkar forcing set DFS5, Grenoble,
600 France: LGGE, 2016.

601 Ferry, N., Parent, L., Garric, G., Barnier, B., and Jourdain, N.C.: Mercator global eddy permitting
602 ocean reanalysis GLORYS1V1: Description and results. *Mercator-Ocean Quarterly Newsletter*,
603 36, 15-27, 2010.

604 Fichet, T., and Maqueda, M.A.M.: Sensitivity of a global sea ice model to the treatment of ice
605 thermodynamics and dynamics. *Journal of Geophysical Research: Oceans*, 102(C6), 12609-
606 12646, 1997.

607 Fischer, J., Visbek, M., Zantopp, R., Nunes, N.: Interannual to decadal variability of outflow from
608 the Labrador Sea. *Geophysical Research Letters*, 37(24), 2010.

609 Frajka-Williams, E., Rhines, P.B., and Eriksen, C.C.: Horizontal stratification during deep
610 convection in the Labrador Sea. *Journal of Physical Oceanography*, 44(1), 220-228, 2014.

611 Fratantoni, P.S. and Pickart, R.S.: The Western North Atlantic Shelfbreak Current System in
612 Summer. *Journal of Physical Oceanography*, 37(10), 2509-2533, 2007.

613 Fresnay, S., Ponte, A.L., Le Gentil, S., Le Sommer, J.: Reconstruction of the 3-D dynamics from
614 surface variable in a high-resolution simulation of the North Atlantic. *Journal of Geophysical
615 Research: Oceans*, 123(3), 1612-1630, 2018.

616 Garcia-Quintana, Y., Courtois, P., Hu, X., Pennelly, C., Kieke, D., and Myers, P.G.: Sensitivity of
617 Labrador Sea Water formation to changes in model resolution, atmospheric forcing, and
618 freshwater input. *Journal of Geophysical Research: Oceans*, 124(3), 2126-2152, 2019.

619 Gelderloos, R., Katsman, C.A. and Drijfhout, S.S.: Assessing the roles of three eddy types in
620 restratifying the Labrador Sea after deep convection. *Journal of Physical Oceanography*, 41(11),
621 2102-2119, 2011.

622 Gordon, A.L., Visbeck, M., and Comiso, J.C.: A possible link between the Weddell Polynya and
623 the Southern Annular Mode. *Journal of Climate*, 20(11), 2558-2571, 2007.

624 Hansen, B., and Østerhus, S.: North Atlantic-Nordic Seas exchanges. *Progress in Oceanography*,
625 45(2), 109-208, 2000.

626 Hátún, H., Eriksen, C.C., and Rhines, P.B.: Buoyant eddies entering the Labrador Sea observed
627 with gliders and altimetry. *Journal of Physical Oceanography*, 37(12), 2838-2854, 2007.

628 Holte, J., and Talley, L.: A new algorithm for finding mixed layer depths with applications to
629 Argo data and Subantarctic Mode Water formation. *Journal of Atmospheric and Oceanic*
630 *Technology*, 26(9), 1920-1939, 2009.

631 Kieke, D., Klein, B., Stramma, L., Rhein, M., and Koltermann, K.P.: Variability and propagation of
632 Labrador Sea Water in the southern subpolar North Atlantic. *Deep Sea Research Part I:*
633 *Oceanographic Research Papers*, 56(10), 1656-1674, 2009.

634 Lab Sea Group: The Labrador Sea deep convection experiment. *Bulletin of the American*
635 *Meteorological Society*, 79(10), 2033-2058, 1998.

636 Large, W.G., and Yeager, S.G.: The global climatology of an interannually varying air-sea flux
637 data set. *Climate Dynamics*, 33(2-3), 341-364, 2008

638 Latif, M., Roechner, E., Mikolajewicz, U., and Voss, R.: Tropical stabilization of the thermohaline
639 circulation in a greenhouse warming simulation. *Journal of Climate*, 13(11), 1809-1813, 2000.

640 Lazier, J., Hendry, R., Clarke, A., Yashayaev, I., and Rhines, P.: Convection and restratification in
641 the Labrador Sea, 1990-2000. *Deep Sea Research Part I: Oceanographic Research Papers*,
642 49(10), 1819-1835, 2002.

643 Lazier, J.R.N., and Wright, D.G.: Annual velocity variations in the Labrador Current, *Journal of*
644 *Physical Oceanography*, 23(4), 659-678, 1993.

645 Lilly, J.M., Rhines, P.B., Visbeck, M., Davis, R., Lazier, J.R.N., Schott, F., and Farmer, D.: Observing
646 deep convection in the Labrador Sea during winter 1994/95. *Journal of Physical Oceanography*,
647 29, 2065-2098, 1999.

648 Lilly, J.M., Rhines, P.B., Schott, F., Lavender, K., Lazier, J., Send, U., and D'Asaro, E.:
649 Observations of the Labrador Sea eddy field. *Progress in Oceanography*, 59(1), 75-176, 2003.

650 Lin, P., Pickart, R.S., Torres, D.J., and Pacini, A.: Evolution of the freshwater coastal current at
651 the southern tip of Greenland. *Journal of Physical Oceanography*, 48(9), 2127-2140, 2018

652 Madec, G.: Note du Pôle de modélisation. Institut Pierre-Simon Laplace (IPSL), France, No 27,
653 ISSN No 1288-1619, 2008.

654 Marshall, J. and Schott, F.: Open-ocean convection: Observations, theory, and models. *Reviews*
655 *of Geophysics*, 37(1), 1-64, 1999.

656 Marzocchi, A., Hurshi, J.J.M., Holiday, N.P., Cunningham, S.A., Blaker, A.T., and Coward, A.C.:
657 The North Atlantic subpolar circulation in an eddy-resolving global ocean model. *Journal of*
658 *Marine Systems*, 142, 126-143, 2015.

659 McGeehan, I. and Maslowski, W.: Impact of shelf-basin freshwater transport on deep
660 convection in the western Labrador Sea. *Journal of Physical Oceanography*, 41(11), 2187-2210,
661 2011.

662 Müller, V., Kieke, D., Myers, P.G., Pennelly, C., and Mertens, C.: Temperature flux carried by
663 individual eddies across 47° in the Atlantic Ocean. *Journal of Geophysical Research: Oceans*,
664 122(3), 2441-2464, 2017.

665 Müller, V., Kieke, D., Myers, P.G., Pennelly, C., Steinfeldt, R., and Stendardo, I.: Heat and
666 freshwater transport by mesoscale eddies in the southern subpolar North Atlantic. *Journal of*
667 *Geophysical Research: Oceans*, 124(8), 5565-5585, 2019.

668 Myers, P.: Impact of freshwater from the Canadian Arctic Archipelago on Labrador Sea water
669 formation. *Geophysical Research Letters*, 32(6), 2005.

670 Pennelly, C.: A 1/60 degree NEMO configuration within the Labrador Sea: LAB60, Zenodo,
671 <http://doi.org/10.5281/zenodo.3762748>, 2020.

672 Pennelly, C. Hu, X., and Myers, P.G.: Cross-isobath freshwater exchange within the North
673 Atlantic Subpolar Gyre. *Journal of Geophysical Research: Oceans*, 124(10), 6831-6853, 2019.

674 Rattan, S., Myers, P.G., Treguier, A.M., Theetten, S., Biastoch, A., and Böning, C. Towards an
675 understanding of Labrador Sea salinity drift in eddy-permitting simulations. *Ocean Modelling*,
676 35(102), 77-88, 2010.

- 677 Rieck, J.K., Böning, C.W., and Getzlaff, K.: The nature of eddy kinetic energy in the Labrador Sea:
678 Different types of mesoscale eddies, their temporal variability, and impact on deep convection.
679 *Journal of Physical Oceanography*, 49(8), 2075-2094, 2019.
- 680 Schmidt, S. and Send, U.: Origin and composition of seasonal Labrador Sea freshwater. *Journal*
681 *of Physical Oceanography*, 37(6), 1445-1454, 2007.
- 682 Schulze, L.M., Pickart, R.S., and Moore, G.W.K.: Atmospheric forcing during active convection in
683 the Labrador Sea and its impact on mixed-layer-depths. *Journal of Geophysical Research:*
684 *Oceans*, 121(9), 6978-6992, 2016.
- 685 Smith, G.C., Roy, F., Mann, P., Dupont, F., Brasnett, B., Lemieux, J.F., Laroche, S., and Bélair, S.:
686 A new atmospheric dataset for forcing ice-ocean models: Evaluation of reforecasts using the
687 Canadian global deterministic prediction system. *Quarterly Journal of the Royal Meteorological*
688 *Society*, 140(680), 881-894, 2014.
- 689 Straneo, F.: Heat and freshwater transport through the central Labrador Sea. *Journal of Physical*
690 *Oceanography*, 36(4), 606-628, 2006.
- 691 Straneo, F. and Saucier, F.: The arctic-subarctic exchange through Hudson Strait. *Arctic-*
692 *Subarctic Ocean Fluxes*, Springer, Dordrecht, 249-261, 2008.
- 693 De Steur, L., Hansen, E., Gerdes, R., Karcher, M., Fahrbach, E., Holfort, J.: Freshwater fluxes in
694 the East Greenland Current: A decade of observations. *Geophysical Research Letters*, 36(23),
695 2009.
- 696 Su, Z., Wang, J., Klein, P., Thompson, A.F., and Menemenlis, D.: Ocean submesoscales as a key
697 component of the global heat budget. *Nature communications*, 9(1), 1-8, 2018.
- 698 Tréquier, A.M., Theetten, S., Chassignet, E.P., Penduff, T., Smith, R., Talley, L., Beismann, J.O.,
699 and Böning, C.: The North Atlantic subpolar gyre in four high-resolution models. *Journal of*
700 *Physical Oceanography*, 35(5), 757-774, 2005.
- 701 Yashayaev, I. and Loder, J.W.: Recurrent replenishment of Labrador Sea Water and associated
702 decadal-scale variability. *Journal of Geophysical Research: Oceans*, 121(11), 8095-8814, 2016.
- 703 Yashayaev, I.: Hydrographic changes in the Labrador Sea, 1960-2005. *Progress in*
704 *Oceanography*, 73(3-4), 242-276, 2007.

705 Whitworth, T. and Orsi, A.H.: Antarctic Bottom Water production and export by tides in the
 706 Ross Sea. *Geophysical Research Letters* 33(12), 2006.
 707 Zalesak, S.T.: Fully multidimensional flux-corrected transport algorithms for fluids. *Journal of*
 708 *computational physics*, 31(3), 335-362, 1979.

709

710 Tables

711

712 Table 1: Domain settings for the ANHA4 parent domain, SPG12 and LAB60 nested domains.

713 Other settings which are invariant to the domain are shown in Table 2.

Setting	ANHA4	SPG12	LAB60
Horz. Resolution	1/4°	1/12°	1/60°
X points	544	724	1179
Y points	800	694	2659
Timestep [s]	720	240	48
Horiz. Eddy Viscosity [$\text{m}^4 \text{s}^{-1}$]	1.5×10^{11}	1.5×10^{10}	3.5×10^8
Horiz. Eddy Diffusivity [$\text{m}^2 \text{s}^{-1}$]	300	50	20
Lateral Slip Conditions	Free slip	Free slip	No slip

714

715

716

717

718

719

720

721

722

723

724

725

726

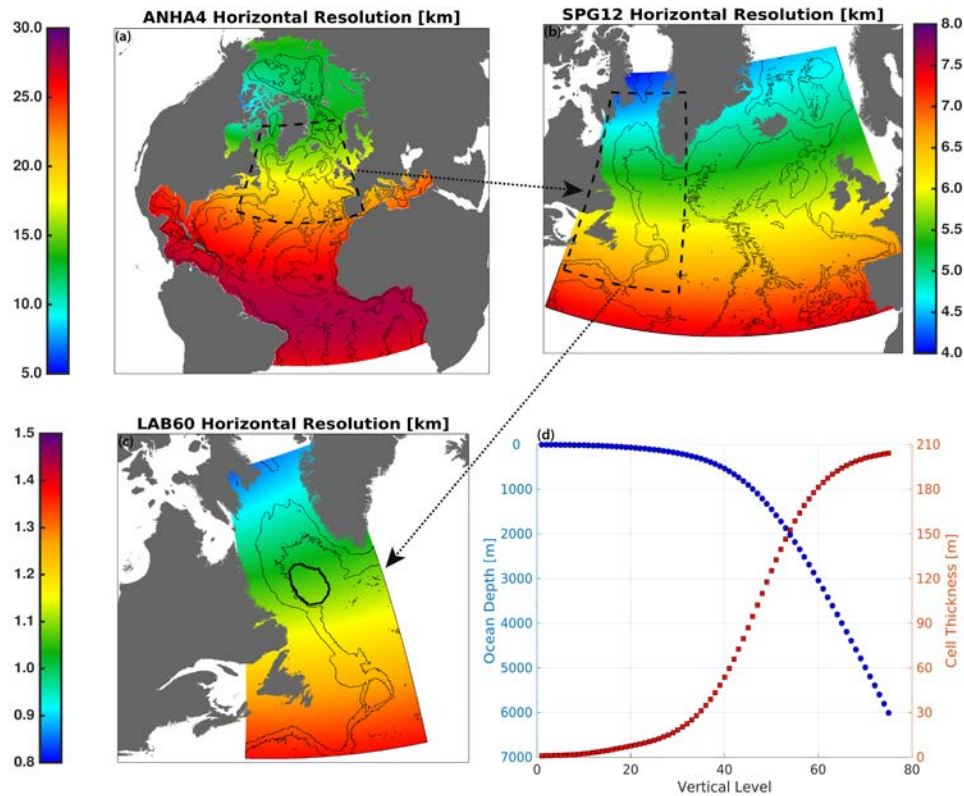
727 Table 2: Model configuration settings which are identical between all three domains. **Bold**
 728 values indicate values which were changed when we migrated LAB60 from the Graham cluster
 729 to Niagara.

Configuration Setting	Value
Vertical grid	75 geopotential levels
Sea-ice model	LIM 2 (Fichefet and Maqueda, 1997)
Bulk formula	CORE (Large and Yeager, 2008)
Liquid discharge	Dia et al. (2009) + Bamber (2012: Greenland)
Solid discharge	Input as liquid
Surface Restoring	None
Initial conditions	Glorys1v1 (T,S,U,V,SSH,ice)
Open boundary conditions	Glorys1v1 (T,S,U,V,ice)
Atmospheric forcing:	
	2002-2006 CGRF (Smith et al, 2014)
	2007-2017 Drakkar Forcing Set 5.2 (Dussin et al. 2016)
Lateral momentum	Bilaplacian operator
Lateral diffusion	Laplacian operator
Vertical eddy viscosity	$1 \times 10^{-4} \text{ m}^2 \text{ s}^{-1}$
Vertical eddy diffusivity	$1 \times 10^{-5} \text{ m}^2 \text{ s}^{-1}$
Mixed layer scheme	Holte and Talley (2009)
Bottom friction	Nonlinear
Hydrostatic approximation	Yes
Passive tracers	Three (see Figure 2)
CPU requested	672 (3000), Broadwell 2.1 GHz (Skylake 2.4 GHz)
Time to complete 1 year	Approximately 700 (200) hours
Initialization date	January 1st, 2002

730

731

732 Figures



733

734

735

736

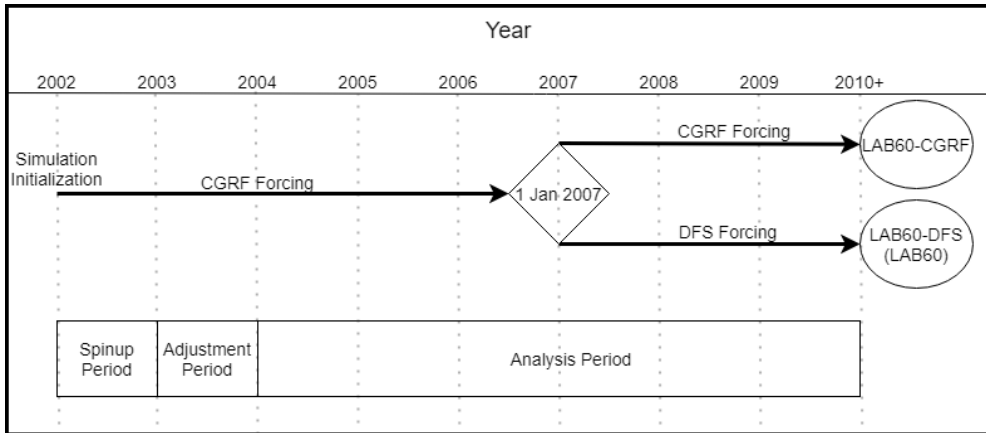
737

738

739

740

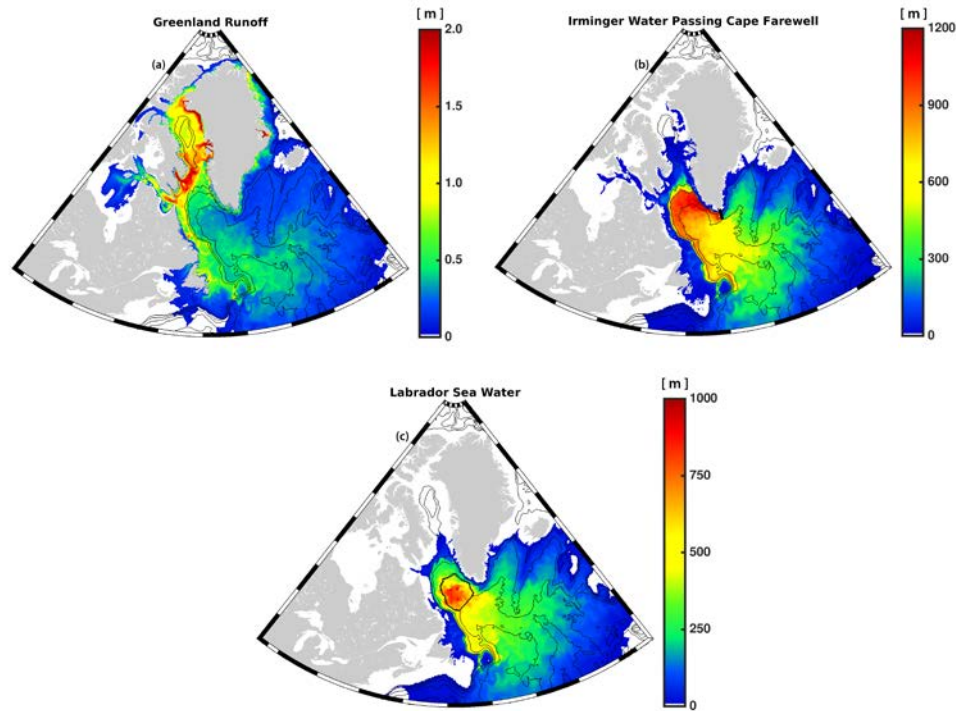
Figure 1: Domain setup for the (a) ANHA4 parent domain, (b) the SPG12 nest, and (c) the LAB60 nest. Horizontal grid resolution, in km, is identified by color. All domains share identical vertical grid structure (d). The thick black contour in (c) identifies a region of interest where calculations of LSW's density, thickness, and mixed layer depth are determined. The 1000m, 3000m, and 5000m isobaths are shown via the thin black contours.



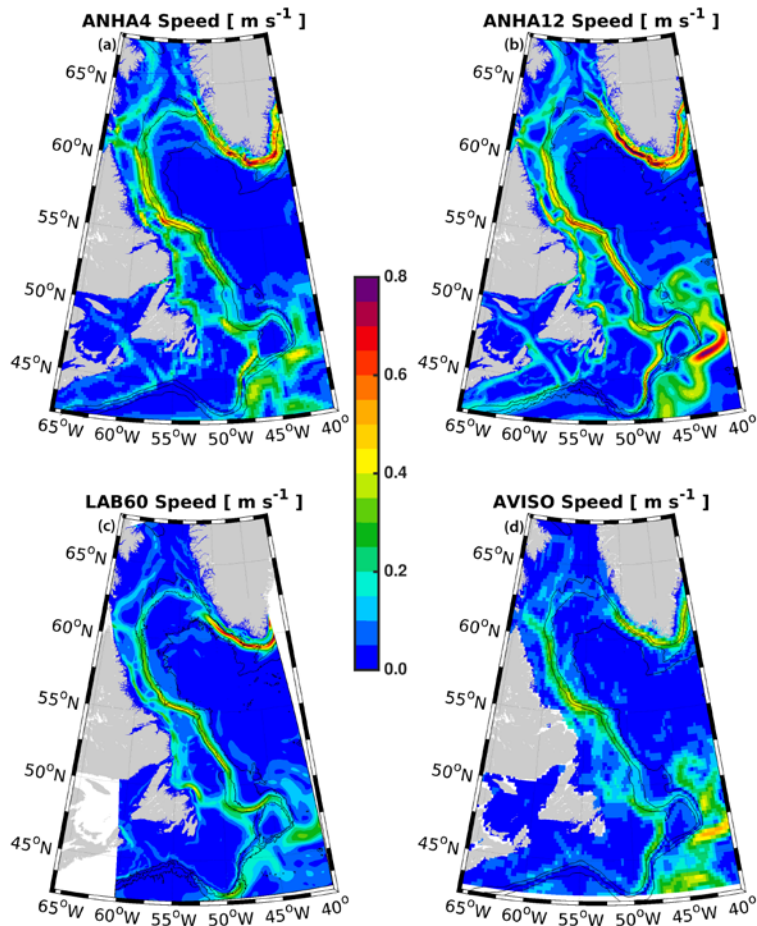
741

742 Figure 2: Diagram showing the multiple periods of the LAB60 simulation. The original simulation
 743 was initialized with CGRF atmospheric forcing in 2002, although a branch swapping to DFS
 744 occurred at the start of 2007. This DFS branch is what is primarily presented in this study.

745



746
 747 Figure 3: The three passive tracers used within our LAB60 simulation with source regions
 748 indicated by thick black lines: (a) Greenland runoff, (b) Irminger Water ($T > 3.5^{\circ}\text{C}$, $S > 34.88$)
 749 which flows west past Cape Farwell, and (c) Labrador Sea Water ($\sigma_{\theta} > 27.68 \text{ kg m}^{-3}$) produced
 750 each convective season. Images are from the simulation date 1 Jan 2010. Bathymetric contours
 751 are every 1000m. Units are the thickness, in meters, of the tracer. Note: as all three domains
 752 are included in this figure, spatial resolution changes within each subfigure.



753

754 Figure 4: Top 50m average speed (2004-2013) for the (a) ANHA4, (b) ANHA12, (c) and LAB60
755 simulations, as well as (d) from AVISO observations. The 1000, 2000, and 3000m isobaths are
756 shown by the black contour lines.

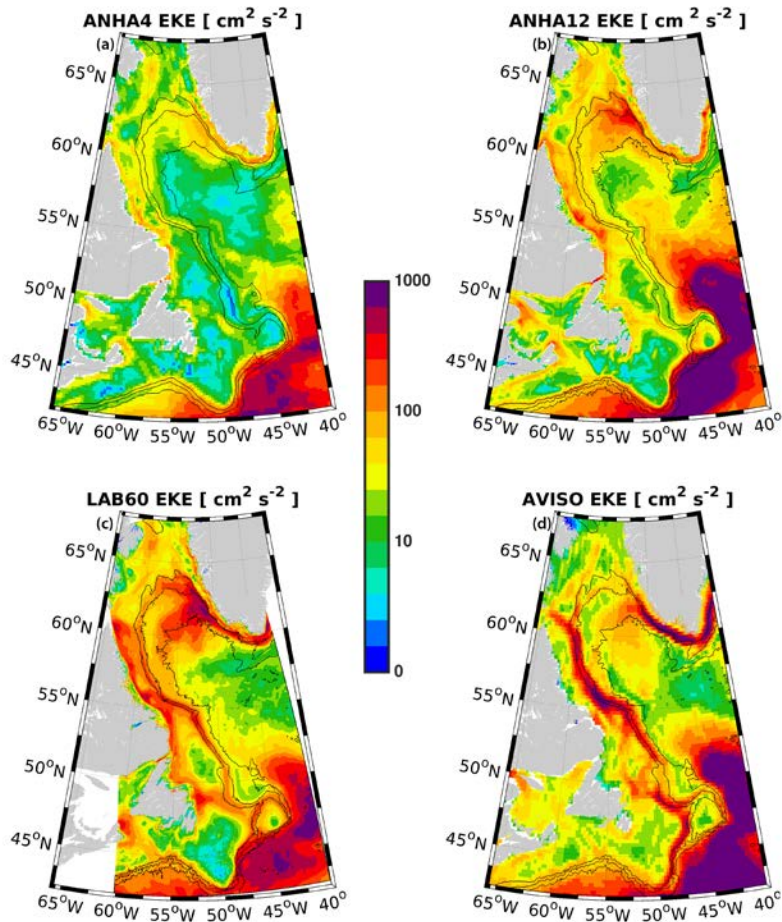
757

758

759

760

761



762

763 Figure 5: Eddy kinetic energy (EKE), as calculated from geostrophic velocities resulting from the

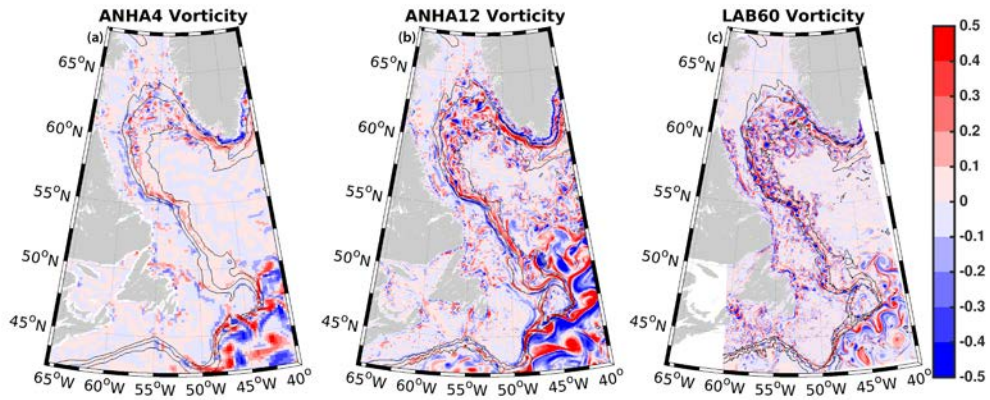
764 sea level height anomaly, are shown for (a) ANHA4, (b) ANHA12, and (c) our LAB60 simulation,

765 from 2004 to 2013. Observations via AVISO are identified in (d). The 1000m, 2000m, and 3000m

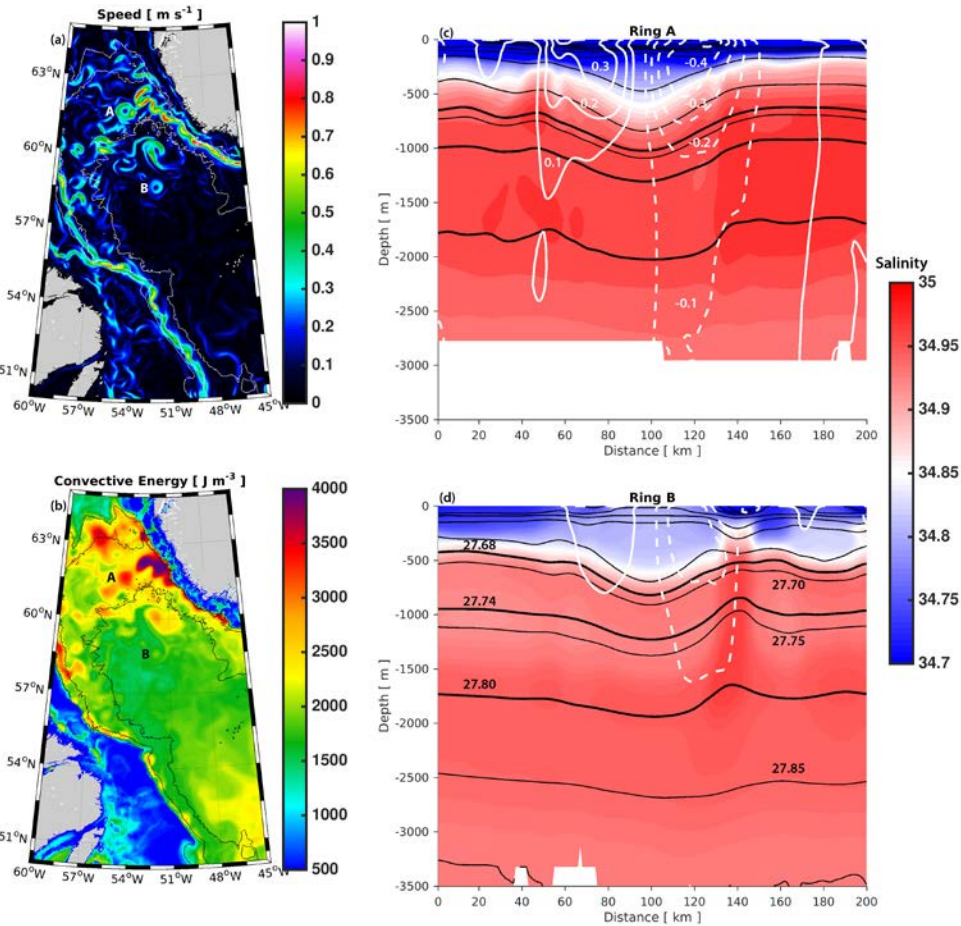
766 isobaths are shown by the black contour lines. A log scale was used for clarity.

767

768



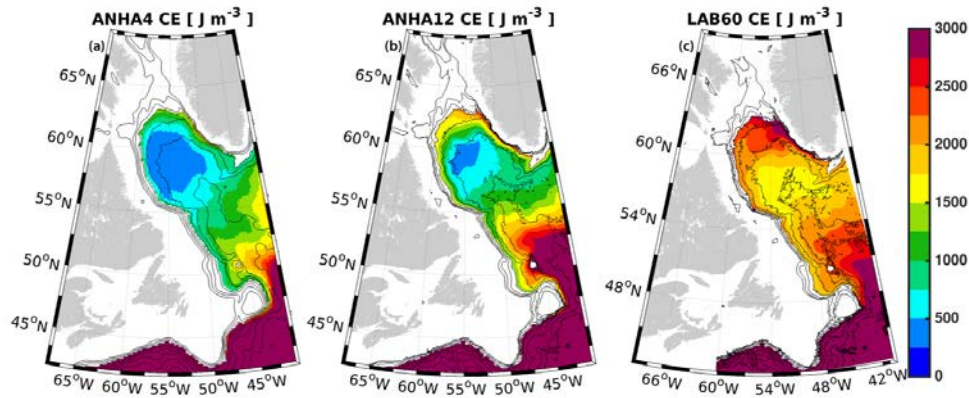
769
770 Figure 6: Top 50m relative vorticity, normalized by the planetary vorticity, as simulated by (a)
771 ANHA4, (b) ANHA12, and (c) LAB60 on 16 March 2008. The 1000m, 2000m, and 3000m isobaths
772 are shown by the black contour lines.
773



774

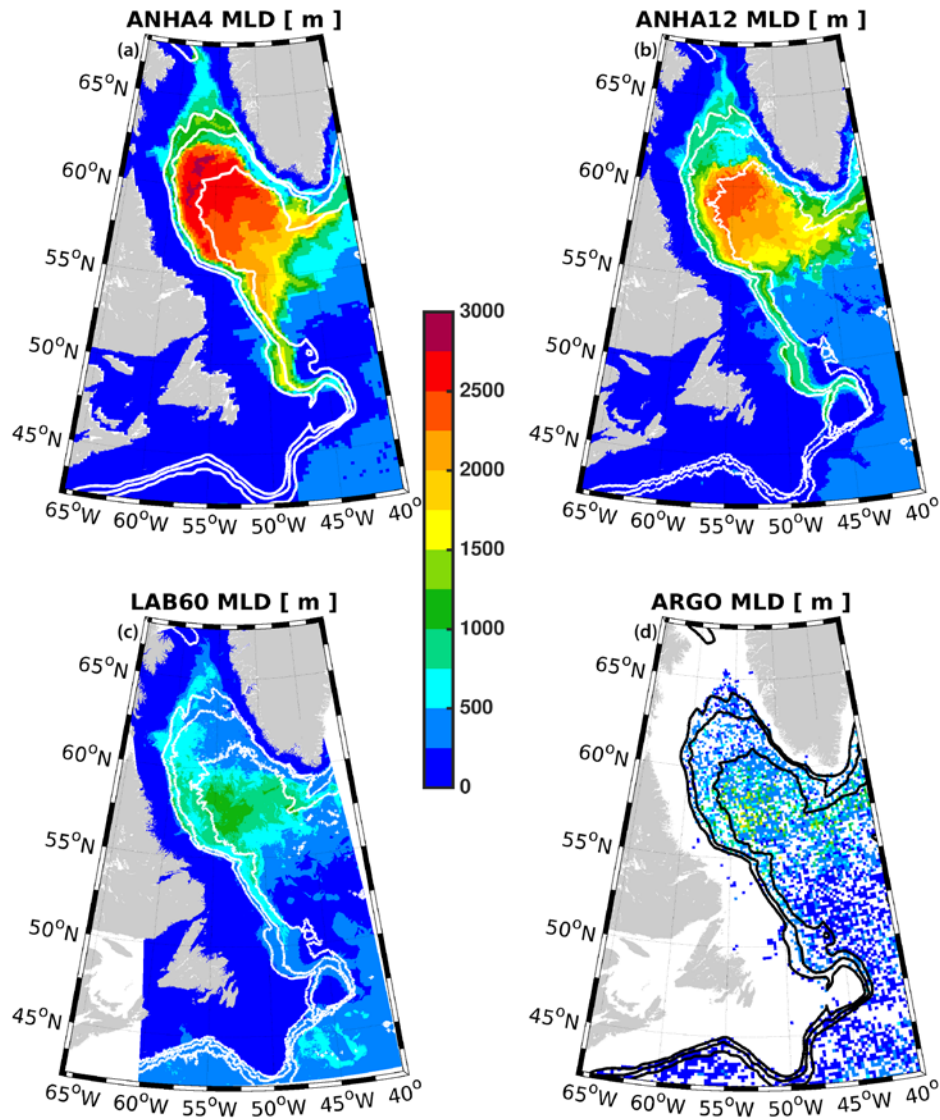
775 Figure 7: LAB60 snapshot (26 July 2007) of the surface speed (a) and convective energy (b)
 776 within the Labrador Sea. Two Irminger Rings are identified by their age with letters: Ring A is a
 777 young Irminger Ring, while Ring B is comparatively older. An east-west cross section through
 778 each of these Irminger Rings is shown in (c) and (d) where colors indicate salinity, black
 779 contours indicate potential density using a contour interval of 0.05 kg m^{-3} , and white contours
 780 indicate meridional velocity where southern flow is dashed and northern flow is solid, using a
 781 contour interval of 0.1 m s^{-1} . Thick black contours indicate the potential density classification of
 782 Upper Labrador Sea Water ($\sigma_\theta=27.68$ to 27.74 kg m^{-3}) and Classical Labrador Sea Water ($\sigma_\theta=$
 783 27.74 to 27.80 kg m^{-3}).

Deleted:



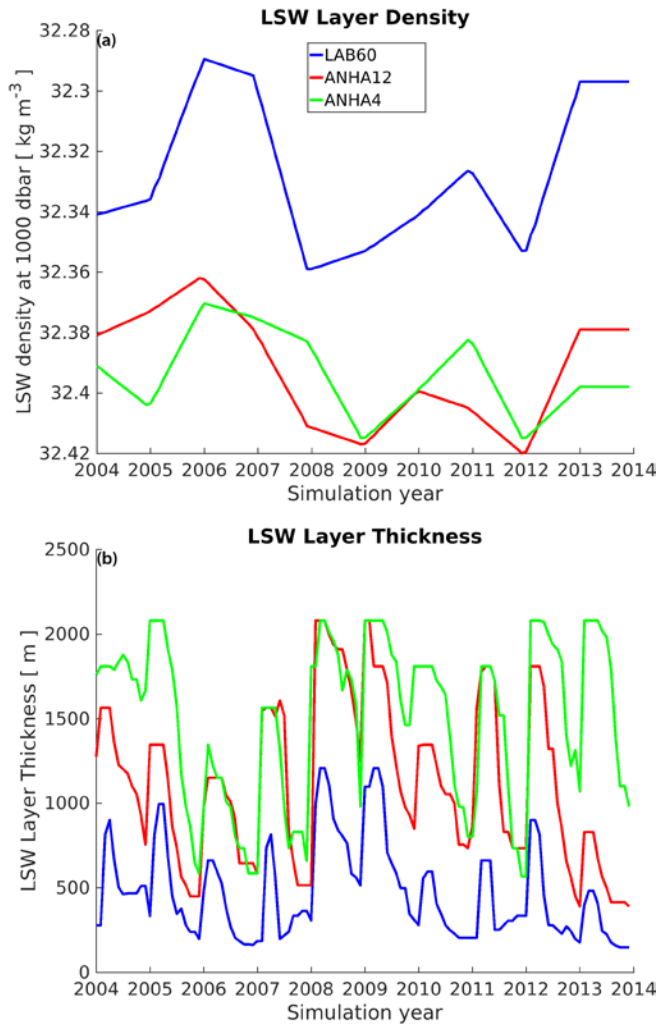
785

786 Figure 8: Convective energy (CE), the strength of stratification down to a reference depth of
787 2000m, is shown for (a) ANHA4, (b) ANHA12, and (c) LAB60. Convective energy was averaged
788 from 2004 through 2013. Values where the depth of the seafloor was less than 2000m were
789 removed to preserve clarity. Bathymetric contours (black lines) are shown every 500m.



790
 791 Figure 9: Maximum mixed layer depth for (a) ANHA4, (b) ANHA12, (c) LAB60, as well as (d)
 792 ARGO observations, where available, from 2004 through the end of 2013. For clarity, the ARGO
 793 data were placed on the same grid as ANHA4. The 1000m, 2000m, and 3000m isobaths are
 794 shown via the white and black contours

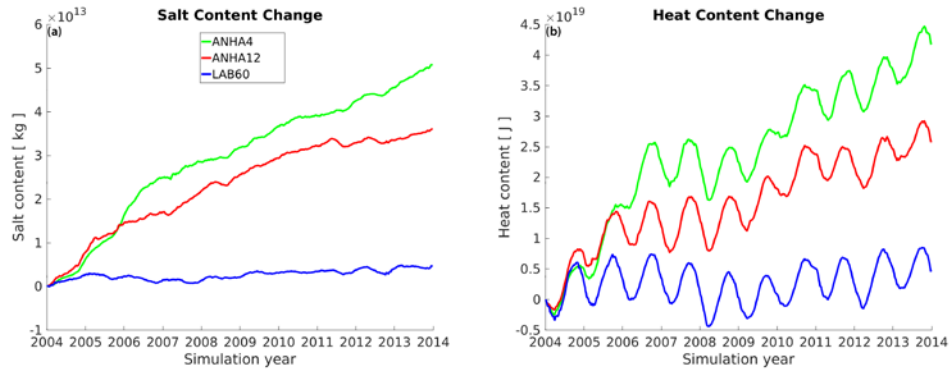
795



796

797 Figure 10: Labrador Sea Water (LSW) density (a) and thickness (b) for the LAB60, ANHA12, and
 798 ANHA4 configurations. LSW density was determined from the thickest layer where a 0.001 kg
 799 m^{-3} change in potential density (ref: 1000 dbar) occurred within the black polygon outlines in
 800 Fig 1c. The LSW layer was then calculated between this density and one which was 0.02 kg m^{-3}
 801 less dense.

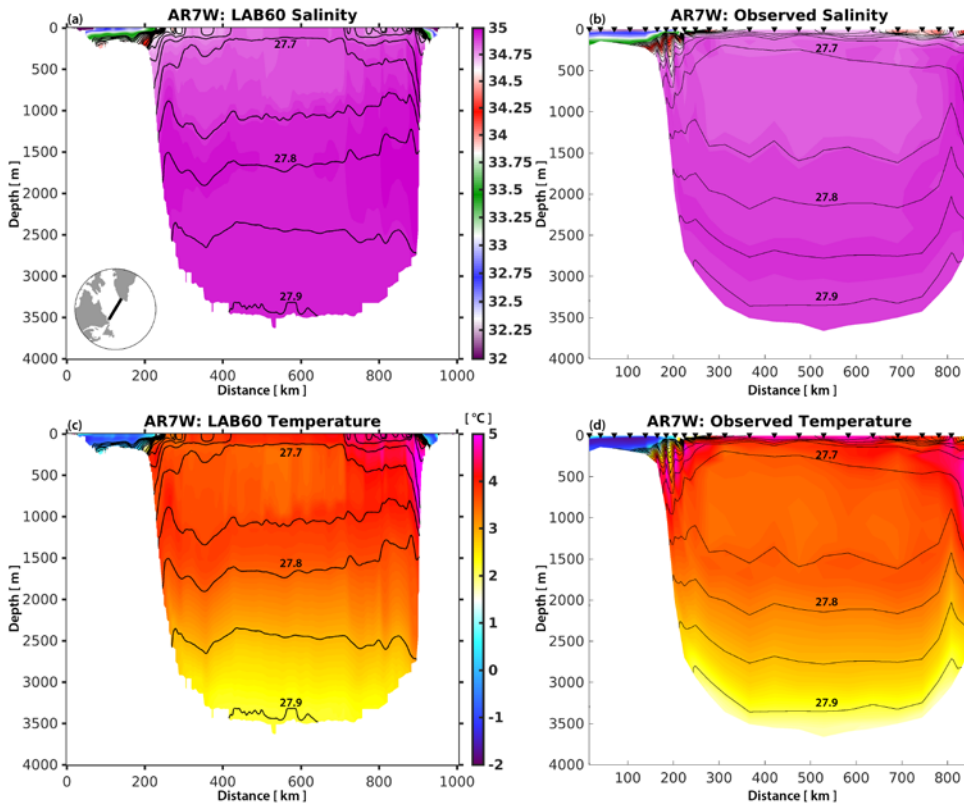
802



803

804 Figure 11: Numerical salt (a) and heat (b) drift in our three simulations as they evolve since 1
805 Jan 2004. Salt and heat content is calculated over the full ocean column within the polygon in
806 Fig. 1c.

807



808

809 Figure 12: Salinity (top) and temperature (bottom) section across AR7W as determined by the
 810 LAB60 simulation (left) and observations (right) from May 2008. Downward triangles identify
 811 collection sites across the AR7W transit carried out by the CCGS Hudson. Potential density
 812 (black contours) isopycnal interval is 0.05 kg m^{-3} .